JOURNAL OF GEOPHYSICAL RESEARCH, VOL. ???, XXXX, DOI:10.1029/,

Nonlinear pitch-angle scattering of relativistic electrons by EMIC waves in the inner magnetosphere

Yoshiharu Omura[1] and Qinghua Zhao,[1]

[1] Research Institute for Sustainable Humanosphere, Kyoto University, Kyoto Japan.

Yoshiharu Omura, Research Institute for Sustainable Humanosphere, Kyoto University, Uji, Kyoto, 611-0011, Japan. (omura@rish.kyoto-u.ac.jp)

Qinghua Zhao, Research Institute for Sustainable Humanosphere, Kyoto University, Uji, Kyoto, 611-0011, Japan. (zhao@rish.kyoto-u.ac.jp)

Abstract. We derive the second-order resonance condition for interaction between a relativistic electron and a coherent Electromagnetic Ion Cyclotron (EMIC) wave with a variable frequency. We perform test particle simulations of relativistic electrons interacting with EMIC waves with a fixed frequency and a rising-tone frequency such as EMIC triggered emissions observed in the inner magnetosphere. Trapping of resonant electrons leads to rapid and efficient pitch-angle scattering of relativistic electrons, resulting in bursty precipitation of relativistic electrons. The efficiency of the pitch-angle scattering depends on the gradient of the magnetic field, the frequency sweep rate, and the wave amplitude. The effective wave trapping occurs for a wide range of pitch angles from 10 to 60 degrees. The most effective pitch-angle scattering takes place for the case of a rising-tone emission with an enhanced magnetic field gradient. Since the efficiency of pitch-angle scattering also depends on the wave amplitude, resonant electrons may not be scattered into the loss cone in a single passage through the wave packet. However, repeated interactions with a series of wave packets result in scattering of relativistic electrons into the loss cone.

1. Introduction

A recent spacecraft observation has revealed coherent and nonlinear characteristics of electromagnetic ion cyclotron (EMIC) waves in the magnetosphere [*Pickett et al.*, 2010]. Coherent waves with rising-tone frequencies are triggered from a constant frequency EMIC wave, and they are called EMIC triggered emissions. The emissions are explained by a nonlinear wave growth theory [*Omura et al.*, 2010] which is essentially the same as the nonlinear mechanisms [*Omura et al.*, 2008, 2009; *Omura and Nunn*, 2011; *Nunn and Omura*, 2012] that generate whistler-mode chorus emissions [e.g., *Tsurutani and Smith*, 1974; *Anderson and Kurth*, 1989; *Lauben et al.,* 1998, 2002; *Santolik et al.*, 2003; *Kasahara et al.*, 2009]. EMIC triggered emissions consisting of a series of rising tones are excited near the magnetic equator by energetic protons from several keV to tens of keV injected into the inner magnetosphere. The frequency sweep rate of the wave plays an important role in the nonlinear wave growth near the magnetic equator. EMIC emissions are also reproduced by a hybrid code simulation, and it is found that a substantial amount of the energetic protons are scattered into the loss cone [*Shoji and Omura*, 2011].

Ground and satellite observations show that EMIC waves cause precipitation of ions with energies of tens of keV and precipitation of relativistic electrons into an isolated proton aurora at the same time [*Miyoshi et al.*, 2008]. The Finnish pulsation magnetometer chain and riometer chain also confirmed the link between the EMIC waves and intense relativistic electron precipitation [*Rodger et al.*, 2008].

A theoretical and numerical analysis of EMIC wave-electron interaction was performed by *Albert and Bortnik* [2009]. They assumed an EMIC wave with a constant frequency

in analyzing the nonlinear interaction. In the present study, we include effects of the variable frequencies of the EMIC triggered emissions in deriving the second-order cyclotron resonance condition and in performing test particle simulations.

We first derive the second-order resonance condition of a relativistic electron interacting with an EMIC wave with a variable frequency in section 2. Theoretical analyses of the minimum resonance energy, nonlinear wave trapping, and associated pitch-angle scattering are also presented. In section 3, we study the nonlinear dynamics of relativistic electrons interacting with the EMIC wave by test particle simulations with various cases of different wave amplitudes, frequency variations, and magnetic field curvatures near the equator. In section 4, we present the summary and discussion.

2. Nonlinear Dynamics of Relativistic Electrons

We assume a coherent electromagnetic wave propagating parallel to a static magnetic field B_0 directed along the z-axis, and z is the distance along the magnetic field line from the magnetic equator. The wave fields are in the transverse plane containing x- and y-axes as shown in Figure 1. We express the wave magnetic field vector in the transverse plane by a complex form $\vec{B}_w = B_w \exp(i\psi)$. We assume an electron moving along the z-axis with a parallel velocity $v_\parallel$ and a perpendicular velocity $\vec{v}_\perp = v_\perp \exp(i\phi)$, where we define the phase ϕ in the direction of the electron cyclotron motion. Assuming an L-mode EMIC wave propagating in the positive z direction, we define the frequency ω and the wavenumber k by

$$\omega = -\frac{\partial \psi}{\partial t} , \qquad k = \frac{\partial \psi}{\partial z} \quad . \tag{1}$$

The relativistic equation of motion is given by

$$m_0 \frac{\mathrm{d}(\gamma v)}{\mathrm{d}t} = -e[E_w + v \times (B_0 + B_w)] \quad , \tag{2}$$

where m_0 is the electron rest mass. The γ is the Lorentz factor given by

$$\gamma = \frac{1}{\sqrt{1-(v/c)^2}} \quad , \tag{3}$$

where c is the speed of light. Since an electron undergoes cyclotron motion with a cyclotron radius $r_c = \gamma v_\perp / \Omega_e$, where $\Omega_e = eB_z/m_0$, the nonuniform magnetic field B_0 has a radial component $B_r = -(r_c/2)(\partial B_z/\partial z)$ to satisfy $\nabla \cdot B_0 = 0$. The equation of motion (2) is rewritten as

$$\frac{\mathrm{d}(\gamma v_\parallel)}{\mathrm{d}t} = v_\perp \Omega_w \sin\zeta - \frac{\gamma v_\perp^2}{2\Omega_e}\frac{\partial \Omega_e}{\partial z} \quad , \tag{4}$$

$$\frac{\mathrm{d}(\gamma \vec{v}_\perp)}{\mathrm{d}t} = \left[\left(\frac{\omega}{k} - v_\parallel\right)\Omega_w \sin\zeta + i\left(\frac{\omega}{k} - v_\parallel\right)\Omega_w \cos\zeta + \frac{\gamma v_\parallel v_\perp}{2\Omega_e}\frac{\partial \Omega_e}{\partial z} + i v_\perp \Omega_e\right]\exp(i\phi) \quad , \tag{5}$$

where $\Omega_w = eB_w/m_0$, $\zeta = \phi - \psi$, and we made use of $E_w = (\omega/k)B_w$ from Maxwell's equations. Noting that the left-hand side of (5) is expanded as

$$\frac{\mathrm{d}(\gamma \vec{v}_\perp)}{\mathrm{d}t} = \frac{\mathrm{d}(\gamma v_\perp)}{\mathrm{d}t}\exp(i\phi) + i\gamma v_\perp \frac{\mathrm{d}\phi}{\mathrm{d}t}\exp(i\phi) \quad , \tag{6}$$

we separate the real and imaginary parts of (5) to obtain

$$\frac{\mathrm{d}(\gamma v_\perp)}{\mathrm{d}t} = \left(\frac{\omega}{k} - v_\parallel\right)\Omega_w \sin\zeta + \frac{\gamma v_\parallel v_\perp}{2\Omega_e}\frac{\partial \Omega_e}{\partial z} \quad , \tag{7}$$

$$\frac{\mathrm{d}\phi}{\mathrm{d}t} = \frac{1}{\gamma v_\perp}\left(\frac{\omega}{k} - v_\parallel\right)\Omega_w \cos\zeta + \frac{\Omega_e}{\gamma} \quad . \tag{8}$$

Equations (4), (7), and (8) describe the dynamics of a relativistic electron interacting with the L-mode EMIC wave.

2.1. Second-order Resonance Condition

To study the resonant interaction of an electron with the L-mode EMIC wave, we calculate a time derivative of the relative phase angle $\zeta(t) = \phi(t) - \psi(t, z)$ as seen from a frame of reference moving with the parallel velocity $v_\parallel$ of the electron,

$$\frac{\mathrm{d}\zeta}{\mathrm{d}t} = \frac{\mathrm{d}\phi}{\mathrm{d}t} - (-\omega + v_\parallel k) \quad . \tag{9}$$

Noting that the anomalous cyclotron resonance condition between the EMIC wave and an electron is given by

$$\omega - k v_\parallel = -\frac{\Omega_e}{\gamma} \quad , \tag{10}$$

we define the resonance velocity as

$$V_R = (\omega + \Omega_e/\gamma)/k \quad . \tag{11}$$

Introducing a new variable $\theta = k(v_\parallel - V_R)$, we obtain from (8) and (9)

$$\frac{\mathrm{d}\zeta}{\mathrm{d}t} = -\frac{\Omega_w}{\gamma k v_\perp}\left(\theta + \frac{\Omega_e}{\gamma}\right)\cos\zeta - \theta \quad . \tag{12}$$

Since $\omega << \Omega_e$, we have $V_R \simeq \Omega_e/(\gamma k)$. Assuming $v_\perp \sim V_R$, we have

$$\frac{\mathrm{d}\zeta}{\mathrm{d}t} \sim -\frac{\Omega_w}{\Omega_e}\left(\theta + \frac{\Omega_e}{\gamma}\right)\cos\zeta - \theta \quad . \tag{13}$$

As far as the amplitude is small enough so that $\Omega_w \ll \Omega_e$, the first term on the right-hand side of (13) is negligible, and we find

$$\frac{\mathrm{d}\zeta}{\mathrm{d}t} = -\theta \quad . \tag{14}$$

When $\theta \simeq 0$, i.e., $v_\parallel \simeq V_R$, the first-order phase variation becomes very small, and this is the first-order cyclotron resonance condition.

Assuming $\theta \simeq 0$, we calculate the second-order derivative of the phase ζ,

$$\frac{\mathrm{d}^2\zeta}{\mathrm{d}t^2} = -\frac{\mathrm{d}\theta}{\mathrm{d}t} = k\frac{\mathrm{d}V_R}{\mathrm{d}t} - k\frac{\mathrm{d}v_\parallel}{\mathrm{d}t} \quad , \tag{15}$$

where we have neglected the term containing $\mathrm{d}k/\mathrm{d}t$ because $v_\parallel - V_R \simeq 0$. From (11), we have

$$\frac{\mathrm{d}V_R}{\mathrm{d}t} = \frac{1}{k}\frac{\mathrm{d}\omega}{\mathrm{d}t} + \frac{1}{k}\frac{\mathrm{d}}{\mathrm{d}t}\left(\frac{\Omega_e}{\gamma}\right) - \frac{1}{k^2}\left(\omega + \frac{\Omega_e}{\gamma}\right)\frac{\mathrm{d}k}{\mathrm{d}t} \quad . \tag{16}$$

We need to evaluate the total time derivatives on the right-hand side of (15) in the frame of reference moving with the parallel velocity $v_\parallel$ of the electron.

In calculating the first term of (16), we need the wave equation [*Omura et al.*, 2010],

$$\frac{\partial\omega}{\partial t} + V_g\frac{\partial\omega}{\partial z} = 0 \quad , \tag{17}$$

where V_g is the group velocity given by

$$V_g = 2c^2k\left[\Pi_c + \omega\sum_s \frac{\omega_{ps}^2}{(\Omega_s - \omega)^2}\right]^{-1} \quad . \tag{18}$$

The parameter Π_c is defined by

$$\Pi_c = \sum_s \frac{\omega_{ps}^2}{\Omega_s - \omega} - \frac{\omega_{pe}^2}{\Omega_e} \quad , \tag{19}$$

where Ω_s and ω_{ps} are a cyclotron frequency and a plasma frequency of species "s", respectively, and ω_{pe} is the electron plasma frequency. From the charge neutrality condition, we have

$$\frac{\omega_{pe}^2}{\Omega_e} = \sum_s \frac{\omega_{ps}^2}{\Omega_s} \quad . \tag{20}$$

Using (20), we can rewrite the parameter Π_c as

$$\Pi_c = \omega\sum_s \frac{\omega_{ps}^2}{\Omega_s(\Omega_s - \omega)} \quad . \tag{21}$$

Substituting (21) into (18), we can eliminate the electron parameters from the expression of the group velocity as

$$V_g = \frac{2c^2k}{\omega}\left[\sum_s \frac{\omega_{ps}^2(2\Omega_s - \omega)}{\Omega_s(\Omega_s - \omega)^2}\right]^{-1} \quad . \tag{22}$$

Using (17), we obtain

$$\frac{\mathrm{d}\omega}{\mathrm{d}t} = \left(1 - \frac{v_\parallel}{V_g}\right)\frac{\partial\omega}{\partial t} \quad . \tag{23}$$

We consider the variation of the kinetic energy K of the particle accelerated by the transverse electric field of the wave, which is given by

$$\frac{\mathrm{d}K}{\mathrm{d}t} = eE_w v_\perp \sin\zeta \quad . \tag{24}$$

Noting that $K = m_0c^2(\gamma - 1)$, we find from (24) that

$$\frac{\mathrm{d}\gamma}{\mathrm{d}t} = \frac{\omega\Omega_w v_\perp}{kc^2}\sin\zeta \quad . \tag{25}$$

We obtain the total time derivative in the second term of (16) as

$$\frac{\mathrm{d}}{\mathrm{d}t}\left(\frac{\Omega_e}{\gamma}\right) = \frac{v_\parallel}{\gamma}\frac{\partial\Omega_e}{\partial z} - \frac{\Omega_e\omega\Omega_w v_\perp}{\gamma^2 kc^2}\sin\zeta \quad . \tag{26}$$

Noting that $\partial k/\partial t = -\partial\omega/\partial z$, we calculate the time derivative of k from (17)

$$\frac{\partial k}{\partial t} = \frac{1}{V_g}\frac{\partial\omega}{\partial t} \quad . \tag{27}$$

The spatial derivative of k is calculated from the linear dispersion relation of the EMIC wave [*Omura et al.*, 2010]

$$c^2k^2 = \omega\Pi_c \quad , \tag{28}$$

which is plotted in Figure 2(a), where the frequency ω is normalized by the proton cyclotron frequency Ω_H. Differentiating (28) with respect to z, we obtain

$$\frac{\partial k}{\partial z} = -\frac{1}{V_g^2}\frac{\partial\omega}{\partial t} + \frac{\omega}{\Omega_e}\left(\frac{\Pi_c}{2c^2k} - \frac{1}{V_g}\right)\frac{\partial\Omega_e}{\partial z} \quad . \tag{29}$$

Noting that $\mathrm{d}k/\mathrm{d}t = \partial k/\partial t + v_\parallel\partial k/\partial z$, we obtain from (27) and (29)

$$\frac{\mathrm{d}k}{\mathrm{d}t} = \frac{1}{V_g}\left(1 - \frac{v_\parallel}{V_g}\right)\frac{\partial\omega}{\partial t} + v_\parallel\frac{\omega}{\Omega_e}\left(\frac{\Pi_c}{2c^2k} - \frac{1}{V_g}\right)\frac{\partial\Omega_e}{\partial z} \quad . \tag{30}$$

Substituting (23), (26), and (30) into (16), we have

$$\frac{\mathrm{d}V_R}{\mathrm{d}t} = \frac{1}{k}\left(1-\frac{V_R}{V_g}\right)^2\frac{\partial\omega}{\partial t} + \left[\frac{V_R}{k\gamma} - \frac{V_R^2\omega}{k\Omega_e}\left(\frac{\Pi_c}{2c^2k} - \frac{1}{V_g}\right)\right]\frac{\partial\Omega_e}{\partial z} - \frac{\Omega_e\omega\Omega_w v_\perp}{(\gamma kc)^2}\sin\zeta \quad , \tag{31}$$

where we set $v_\parallel = V_R = (\omega + \Omega_e/\gamma)/k$.

From (4) and (25), we obtain

$$\frac{\mathrm{d}v_\parallel}{\mathrm{d}t} = \left(1-\frac{\omega V_R}{kc^2}\right)\frac{v_\perp\Omega_w}{\gamma}\sin\zeta - \frac{v_\perp^2}{2\Omega_e}\frac{\partial\Omega_e}{\partial z} \quad , \tag{32}$$

where we set $v_\parallel = V_R$ on the right-hand side. Substituting (31) and (32) into (15), we obtain the second-order derivative of ζ as

$$\frac{\mathrm{d}^2\zeta}{\mathrm{d}t^2} = -\omega_{tr}^2(\sin\zeta + S) \quad , \tag{33}$$

where

$$\omega_{tr}^2 = \left(1-\frac{V_p^2}{c^2}\right)\frac{kv_\perp\Omega_w}{\gamma} \quad , \tag{34}$$

$$S = -\frac{1}{\omega_{tr}^2}\left(s_1\frac{\partial\omega}{\partial t} + s_2V_p\frac{\partial\Omega_e}{\partial z}\right) \quad , \tag{35}$$

$$s_1 = \left(\frac{V_R}{V_g} - 1\right)^2 \quad , \tag{36}$$

$$s_2 = \frac{\omega}{\Omega_e}\left(\frac{v_\perp^2 - V_R^2}{2V_p^2} + \frac{V_R^2}{V_gV_p}\right) + \frac{V_R}{\gamma V_p} \quad , \tag{37}$$

and $V_p = \omega/k$. Since $V_p \ll c$ for EMIC waves, $\omega_{tr} \simeq \sqrt{kv_\perp\Omega_w/\gamma}$. The variable S in (33) is the inhomogeneity factor controlling the dynamics of a resonant electron, and its expression given by (35) is one of the key results of the present study.

2.2. Resonance Velocity and Minimum Resonance Energy

Setting $v^2 = V_R^2 + v_\perp^2$ in (3) and substituting it into (11), we obtain the quadratic equation of V_R, and its positive solution is given by

$$V_R = \frac{c^2k^2V_p + \Omega_e\sqrt{(\Omega_e^2 + c^2k^2 - \omega^2)c^2 - (\Omega_e^2 + c^2k^2)v_\perp^2}}{\Omega_e^2 + c^2k^2} \quad . \tag{38}$$

Noting that $\omega \ll \Omega_e$ and $V_p \ll c$, we find that

$$V_R = \frac{\Omega_e}{\sqrt{\Omega_e^2 + c^2 k^2}} \sqrt{c^2 - v_\perp^2} \quad . \tag{39}$$

From (11), we also find the approximate resonance velocity as

$$V_R = \frac{\Omega_e}{\gamma k} \quad . \tag{40}$$

Since the variation of the kinetic energy is negligible, we set

$$v_\parallel^2 + v_\perp^2 \simeq v_0^2 \quad , \tag{41}$$

where v_0 is the initial velocity before the interaction. Using (41), we eliminating $v_\perp$ from (39) to obtain

$$V_R \simeq v_\parallel \sqrt{\frac{1 + [(c^2 - v_0^2)/v_\parallel^2]}{1 + (ck/\Omega_e)^2}} \quad . \tag{42}$$

Noting that $c^2 - v_0^2 = c^2/\gamma^2$ and using (40), we rewrite (42) as

$$V_R \simeq v_\parallel \sqrt{\frac{1 + \gamma^{-2}(c/v_\parallel)^2}{1 + \gamma^{-2}(c/V_R)^2}} \quad . \tag{43}$$

For highly relativistic electrons with $\gamma \gg 1$, the resonance velocity varies according to the variation of $v_\parallel$, namely,

$$V_R \sim v_\parallel \quad . \tag{44}$$

We can evaluate the minimum kinetic energy of electrons that can interact with EMIC waves from the condition that $\sqrt{V_R^2 + v_\perp^2} < c$. From (40), we obtain

$$\gamma > \frac{\Omega_e}{k\sqrt{c^2 - v_\perp^2}} \quad . \tag{45}$$

Substituting (21) and (28) into (45), we can obtain the minimum kinetic energy K_{min} for electrons to interact with the EMIC wave as

$$K_{min} = m_0 c^2 \left\{ \frac{\Omega_e}{\omega} \left[(1 - \frac{v_\perp^2}{c^2}) \sum_s \frac{\omega_{ps}^2}{(\Omega_s - \omega)\Omega_s} \right]^{-1/2} - 1 \right\} \quad . \tag{46}$$

The minimum resonance energy is expressed as a function of the frequency ω. We assume the loss cone angle $\sim$ 6 degrees, which gives the minimum perpendicular velocity of trapped electrons as $v_\perp \sim 0.1c$. Assuming $v_\perp = 0.1c$, we plot the minimum resonance energy in Figure 2(b). As the frequency ω approaches to the cyclotron frequencies of ions, the energy becomes substantially lower than 1 MeV. The EMIC triggered emissions with rising-tone frequencies are capable to scatter electrons of 100 keV $\sim$ a few MeV.

2.3. Nonlinear Resonant Trapping

Noting that $\mathrm{d}\theta/\mathrm{d}t = -\mathrm{d}^2\zeta/\mathrm{d}t^2$, we eliminate the time variable t from (14) and (33) to obtain

$$\theta \mathrm{d}\theta = -\omega_{tr}^2(\sin\zeta + S)\mathrm{d}\zeta \quad . \tag{47}$$

Integrating (47), we obtain the equation for the trajectories of electrons in (θ, ζ) phase space as

$$\theta^2 - 2\omega_{tr}^2(\cos\zeta - S\zeta) = C \quad , \tag{48}$$

where C is a constant for a specific trajectory. We have plotted the trajectories with $S = 0$ and $S = -0.4$ in Figures 3(a) and 3(b), respectively. The first-order and second-order resonance conditions $\mathrm{d}\zeta/\mathrm{d}t = 0$ and $\mathrm{d}^2\zeta/\mathrm{d}t^2 = 0$ are satisfied at phases ζ_0 and ζ_1, respectively. The phase ζ_0, which becomes 0 for $S = 0$, is the stable equilibrium point around which trapped resonant electrons rotate in time. The phase ζ_1, which is π for $S = 0$, represents an unstable saddle point. Substituting the saddle point values ($\theta = 0$, $\zeta = \pi$) into (48), we obtain the equation for the separatrix ,

$$\theta_s(\zeta) = \pm\omega_{tr}\sqrt{2[\cos\zeta - \cos\zeta_1 - S(\zeta - \zeta_1)]} \quad . \tag{49}$$

For $S = 0$, the maximum value of $\theta_s(\zeta)$ gives the trapping velocity $V_{tr} = 2\omega_{tr}/k$. If parallel velocities of relativistic electrons satisfy the condition

$$V_R - V_{tr} < v_{\parallel} < V_R + V_{tr} \tag{50}$$

at the time of encounter with the tail of the EMIC wave packet, the electrons can be trapped by the wave potential.

Once the electron gets into resonance, the resonance velocity itself varies according to the variation of $v_{\parallel}$ as implied by (44). Because of the nonlinear trapping oscillation, both parallel and perpendicular velocities of trapped resonant electrons oscillate with the trapping frequency.

The efficiency of entrapping resonant electrons depends on the S value. When $S \simeq 0$, the majority of the resonant electrons are trapped. If $|S| > 1$, no trapping takes place. A trapped resonant electron goes through the wave packet with much faster velocity than the group velocity of the wave packet, experiencing the variation of the inhomogeneity factor S due to both $\partial\omega/\partial t$ and $\partial\Omega_e/\partial z$. When the EMIC wave propagates away from the equator with a rising-tone frequency, we find $-1 < S < 0$. From the second-order resonance condition $\sin\zeta_0 + S = 0$, we find $0 < \zeta_0 < \pi$.

2.4. Pitch-angle Scattering

Since the phase velocity V_p is much smaller than the resonance velocity V_R, the diffusion curve nearly overlaps with the iso-energy curve [*Gendrin*, 1981], and we can assume that v is nearly constant. Therefore, a resonant electron only changes its pitch angle α in time. Using $v_{\parallel} = v\cos\alpha$ and $v_{\perp} = v\sin\alpha$, we have

$$\frac{\mathrm{d}v_{\parallel}}{\mathrm{d}t} = -v_{\perp}\frac{\mathrm{d}\alpha}{\mathrm{d}t} \quad . \tag{51}$$

From (32) and (51), we obtain

$$\frac{\mathrm{d}\alpha}{\mathrm{d}t} = -\frac{\Omega_w}{\gamma}\sin\zeta + \frac{v_\perp}{2\Omega_e}\frac{\partial\Omega_e}{\partial z} \quad , \tag{52}$$

where we used $V_p \ll c$. Assuming the second-order resonance condition $\mathrm{d}^2\zeta/\mathrm{d}t^2 = 0$ in (33), we have

$$\sin\zeta_0 + S = 0 \quad . \tag{53}$$

Substituting (53) into (52) assuming trapped resonant electrons satisfy $\zeta \sim \zeta_0$ on average, we have

$$\frac{\mathrm{d}\alpha}{\mathrm{d}t} = \frac{\Omega_w}{\gamma}S + \frac{v_\perp}{2\Omega_e}\frac{\partial\Omega_e}{\partial z} \quad . \tag{54}$$

Since $S < 0$, the electrons trapped by the wave are carried to lower pitch angles as they go through the wave packet, which was also found in a test particle simulation by *Albert and Bortnik* [2009]. The second term on the right-hand side of (54) is the effect of the adiabatic variation, while the first term is due to the wave trapping which is rewritten from (35) as

$$\left(\frac{\mathrm{d}\alpha}{\mathrm{d}t}\right)_{wave} = -\frac{1}{kv_\perp}\left(s_1\frac{\partial\omega}{\partial t} + 2s_2V_p\Omega_{e0}az\right) \quad , \tag{55}$$

where we assumed a parabolic magnetic field $B_z = B_{EQ}(1 + az^2)$, and $\Omega_{e0}(= eB_{EQ}/m_0)$ is the electron cyclotron frequency at the magnetic equator.

3. Test Particle Simulations

We performed test particle simulations of relativistic electrons interacting with the EMIC wave. We solve the relativistic equations of motion for electrons assuming a mirror magnetic field geometry and an EMIC wave with a constant amplitude B_w and a rising-tone frequency. Since the numerical model and scheme have already been described in detail by *Omura and Summers* [2006] and *Furuya et al.* [2008], we only describe how to

implement the mirror magnetic field. We calculate the radial component B_r of the mirror magnetic field as seen by an electron with a velocity (v_x, v_y, v_z), where v_z is a component parallel to the magnetic field. From $\nabla \cdot B_0 = 0$, we have

$$B_r = -\frac{r_c}{2}\frac{\partial B_z}{\partial z} e_r \quad , \tag{56}$$

where e_r is a radial unit vector orthogonal to the perpendicular velocity $v_\perp$, and it is expressed for an electron as

$$e_r = \frac{1}{v_\perp}(v_y, -v_x, 0) \quad . \tag{57}$$

Substituting the cyclotron radius $r_c = \gamma v_\perp / \Omega_e$ and (57) into (56), we obtain the mirror magnetic field as

$$B_0 = (B_x, B_y, B_z) = (-\frac{\gamma}{2\Omega_e}\frac{\partial B_z}{\partial z} v_y, \frac{\gamma}{2\Omega_e}\frac{\partial B_z}{\partial z} v_x, B_z) \quad . \tag{58}$$

The EMIC triggered emission with frequencies typically increasing in time is generated in the equatorial region and propagates in the positive z direction along the magnetic field line. We assume the initial profile of the EMIC wave packet with its wave front and tail at z_f and z_t, respectively, as schematically illustrated in Figure 4. The frequencies of the wave front and tail are fixed, and they are respectively defined as ω_f and ω_t. The frequencies between the wave front and tail are interpolated linearly. When $\omega_f < \omega_t$, the wave frequency observed at a fixed position increases similar to a rising-tone emission. For simplicity, we assume the amplitude of the wave packet is constant in space and time. The wave front and tail propagate along the magnetic field with group velocities V_{gf} and V_{gt}, respectively. A resonant electron starts to interact with the wave packet from the tail and exits from the wave front, passing through the wave packet quickly with a parallel velocity $v_\parallel$ much greater than the group velocities.

3.1. Effect of Nonuniform Magnetic Field

We set up the simulation model and parameters to model the observation of an EMIC triggered emission [*Omura et al.*, 2010]. For simplicity, we first assume a wave packet of a fixed frequency 2.8 Hz ($4.25\times10^{-4}\Omega_{e0}$) with a finite length of $1000c/\Omega_{e0}$, which correspond to the duration time about 40 seconds as observed at a fixed point. We injected 0.98 MeV electrons at $z=-10c/\Omega_{e0}$ with positive parallel velocities. The initial values of electrons varies in their pitch angles $30\sim60$ degrees and phase angles of the perpendicular velocities $0\sim360$ degrees with an interval of 1 degree. A total of 11160($=360\times31$) particles are solved for checking the efficiency of pitch-angle scattering through nonlinear wave trapping by the wave packet. Figure 5 shows trajectories of trapped and untrapped electrons in red and blue, respectively, for five different cases (A - E). The left panels show time histories of pitch angles, and the middle panels show trajectories in the $(\zeta-\theta)$ phase space. The right panels show the distribution F of the resonant electrons as a function of an equatorial pitch angle α_{EQ} which is calculated by assuming adiabatic variation along the magnetic field line as

$$\sin\alpha_{EQ}=\sqrt{\frac{B_{EQ}}{B_z(z)}}\sin\alpha \quad , \tag{59}$$

where z is a position of an electron. The initial distribution of electrons is plotted in a dashed line, and the distribution $F(\alpha_{EQ})$ after the interaction with the wave packet is plotted in a solid line in each case. In Case A shown in Figure 5(a) , we assumed a wave packet with a constant amplitude 2.2 nT ($B_w=0.009B_{EQ}$) and a constant frequency 2.8 Hz ($\omega=0.76\Omega_H$), and injected 0.98 MeV electrons. Some particles are trapped by the wave packet as shown in red. We have identified the trapped electrons by checking the equatorial pitch angles α_{EQ}, whose variation is approximately described by (54) without

the adiabatic acceleration term. For each group of electrons with the same initial pitch angle, we checked the variation of the equatorial pitch angle $\Delta\alpha_{EQ}$. If the maximum decrease in pitch angle is 5 degrees or more, that trajectory is plotted in red. If the maximum increase in pitch angle is 1 degree or more, that trajectory is plotted in blue. The trajectories in red clearly show resonant trapping of electrons, as we can confirm in the middle panel of the (ζ, θ) phase plot, which is similar to the simplified theoretical trajectories in Figure 3(a). The trapped electrons are located initially near the equator, and the inhomogeneity factors S of them are close to 0. From (54), we can understand that the pitch-angle scattering of electrons is not significant, and this is confirmed by the electron distribution $F(\alpha_{EQ})$ in the right panel.

We next inject 3.1 MeV electrons into a wave packet with a constant frequency 1.7 Hz ($\omega = 0.46\Omega_H$) in Case B. It is noted from (46) that we need to lower the frequency of the wave to have effective resonance with the higher energy electrons. As the frequency decreases, the wavenumber also decreases because of the dispersion relation plotted in Figure 2(a). The absolute value of S increases because of the decrease of the wavenumber along with the increasing gradient of the magnetic field as the trapped electrons move away from the equator. The deviation of S from 0 causes an asymmetry of the trajectories of trapped electrons in phase ζ as shown in the middle panel of Figure 5(b). The pitch angles decrease efficiently for the higher energy electrons. With the smaller wavenumber and the smaller perpendicular velocity, the pitch angle variation of the trapped resonant electrons increases as understood from (55).

As Case C, we now try another way to increase the pitch-angle scattering by increasing the curvature of the magnetic field, namely, increasing the parabolic coefficient a in (55)

from $0.8 \times 10^{-7}\Omega_{e0}^2/c^2$ to $3.0 \times 10^{-7}\Omega_{e0}^2/c^2$. As shown in Figure 5(c), we find that the trapped resonant electrons are guided to lower pitch angles because of the enhanced gradient of the magnetic field.

3.2. Effect of Rising-tone Frequency

We set the frequency increasing from 1.7 Hz ($\omega = 2.51 \times 10^{-4}\Omega_{e0}$) to 2.8 Hz ($\omega = 4.25 \times 10^{-4}\Omega_{e0}$) corresponding to the EMIC triggered emissions observed by Cluster spacecraft [*Pickett et al.*, 2010]. While the frequency of the wave packet increases, we assume a constant wave amplitude $B_w = 0.009B_{EQ}$ (Case D). As we find in Figure 5(d), the time variation of the frequency has the same effect as the gradient of the magnetic field in scattering the trapped electrons into the lower pitch angles. The first term on the right-hand side of (55) plays an equal or larger role in changing the pitch angle of trapped electrons compared with the second term corresponding to the gradient of the magnetic field.

When we have both enhanced magnetic field gradient and increasing frequency (Case E), the time scale of the electron precipitation becomes shortest as we find in the left panel of Figure 5(e).

As we find in the left panels of all cases in Figure 5, relativistic electrons with the same kinetic energy are trapped at a wide range of pitch angles when they start to interact with the wave packet. This is because the resonance velocity varies in accordance with variation of the parallel velocities of relativistic electrons as expressed by (43).

To check the effect of the wave amplitude on the pitch-angle scattering, we performed simulation runs with a smaller wave amplitude 1.1 nT ($B_w = 0.0045B_{EQ}$) for Cases A, B, C, D, and E compared with the amplitude 2.2 nT ($B_w = 0.009B_{EQ}$) in Figure 5, and

plotted the results in Figure 6. The trapped electrons are scattered in pitch angle down to ~ 10 degrees, and get out of the wave front. After some adiabatic bounce motion between the mirror points, the electrons may interact with another wave packet near the equator. To find whether such electrons with smaller pitch angles are effectively scattered into loss cone or not, we performed another sets of simulations starting from the initial distribution of electrons with pitch angles $10 \sim 30$ degrees, and the results are shown in Figure 7. We assumed the same wave amplitude $B_w = 0.0045 B_{EQ}$ as assumed in the cases of Figure 6. For the electrons with low pitch angles, they may not be called trapped or untrapped, because we do not find oscillations around the stable equilibrium point. However, we can identify from the different phases of electrons as shown in the middle panels of Figure 7. The electrons plotted in red cross the resonance velocity near the same phase of the trapped electrons, and they are scattered to lower pitch angles, while the electrons plotted in blue cross the resonance velocity with the phase of the untrapped resonant electrons being scattered to higher pitch angles. The effective pitch-angle scattering to both lower and higher angles through resonance imply a coherent nonlinear process that electrons with low pitch angles (< 30 degrees) are effectively scattered in pitch angles to lower or higher angles depending on their phases with respect to the transverse wave fields. Some of the resonant electrons in the lower pitch angles are scattered into the loss cone. Therefore, in the presence of continuous EMIC wave emissions at a fixed frequency or a series of triggered rising-tone emissions, MeV electrons are scattered into the loss cone through repeated interactions with the waves. The efficiency is higher for a larger magnetic field curvature near the magnetic equator. Rising-tone emissions are more effective than a constant-frequency wave in scattering resonant electrons into the loss cone.

4. Summary and Discussion

We have derived the second-order resonance condition for a relativistic electrons interacting with an EMIC wave. We find that efficient pitch-angle scattering takes place because of trapping of resonant electrons by an EMIC wave. Trapped electrons are transferred to the lower pitch angles because of the acceleration by the electric field due to the inhomogeneity of the magnetic field and variation of the wave frequency. At the time of triggered rising-tone emissions, we expect that precipitation of MeV electrons with lower energies near 1 MeV is much enhanced. Since the efficiency of pitch-angle scattering depends on the wave amplitude, resonant electrons interacting with a smaller amplitude wave may not be scattered into the loss cone in a single passage through the wave packet. However, repeated interactions with a series of wave packets result in scattering of relativistic electrons into the loss cone, because the efficiency of the pitch-angle scattering is also high near the loss cone as shown in Figure 7.

The wave-particle interaction between EMIC waves and relativistic electrons has been studied numerically in the frame work of the quasilinear theory [e.g., *Summers et al.*, 2007ab; *Jordanova et al.*, 2008; *Liu et al.*, 2010]. For a coherent waves such as EMIC triggered emissions, the effects of the magnetic field gradient $\partial\Omega_e/\partial z$ and the frequency sweep rate $\partial\omega/\partial t$ as expressed by the inhomogeneity factor S in (35) play an critical role in scattering the pitch angles.

We traced trajectories of resonant electrons with initial pitch angles 10, 20, 30, 40, 50, 60, 70 degrees for Case E with the wave amplitude $B_w = 0.009B_{EQ}$, which shows the maximum variation of pitch angles. We plot the time histories of pitch angles α and variation of the kinetic energies ΔK in Figures 8(a) and 8(b), respectively. Trapped electrons in

red as defined in Figure 5 gain energy being scattered to lower pitch angles. Untrapped electrons in blue lose energy as indicated by (24). However, the energy variations are almost negligible compared with the kinetic energy of electrons. It is interesting to note that resonant electrons trapped by a whistler-mode chorus emission are scattered to higher pitch angles with a significant increase of the kinetic energy [*Omura et al.*, 2007].

In this paper, we assumed a wave packet with a constant amplitude. However, in observation [*Omura et al.*, 2010] and the simulation [*Shoji and Omura*, 2011], the wave packets show modulation of the amplitudes. The amplitude modulation may cause detrapping of the trapped resonant electrons, making the pitch-angle scattering less effective. On the other hand the untrapped electrons can be trapped by the increasing amplitude in space. Quantitative evaluation including the amplitude modulation is left as a future study.

EMIC triggered emissions in the hydrogen band can also excite another EMIC wave in the helium band as reported by *Shoji et al.* [2011]. Near the geosynchronous orbit, EMIC waves in the helium band are often observed in association with large solar wind density [*Clausen et al.*, 2011]. Although the characteristics of the helium band interaction should be the same as the hydrogen band, quantitative studies on coherent pitch-angle scattering by the helium band waves are also left as a future study.

The length of the wave packet as the L-mode EMIC wave is limited in space, because the cyclotron frequency increases as the wave packet propagates from the equator to a higher latitude. The wave frequency approaches to the cut-off frequency of the EMIC wave dispersion relation, and the wave is either to be reflected or converted to the R-mode in the oblique propagation. Therefore, the effect of the spatial gradient of the magnetic

field, as it appears in (35), may not be effective enough for pitch-angle scattering. A wave packet with increasing frequency will be more efficient in causing pitch-angle scattering.

Although we have assumed parallel propagation in the present study, the observation by the Cluster spacecraft shows that the wave normal angles fall in the range of 25 to 70 degrees [*Pickett et al.*, 2010]. Effects of the oblique propagation on the pitch-angle scattering are also left as future studies.

Recently, *Wang et al.*, [2012] conducted an interesting experiment of precipitation of relativistic electrons trapped in a mirror magnetic field by a shear Alfvén wave in a laboratory device. It would be interesting to see how the efficiency of the pitch-angle scattering changes by injecting a coherent wave with a varying frequency.

Acknowledgments. This work was supported by Grant-in-Aid 23340147 of the Ministry of Education, Science, Sports and Culture of Japan.

References

Anderson, R. R., and W. S. Kurth (1989), Discrete electromagnetic emissions in planetary magnetospheres, In *Plasma Waves and Instabilities at Comets and in Magnetospheres, Geophys. Monogr. Ser.*, *53*, edited by B. T. Tsurutani and H. Oya, p. 81, AGU, Washington, D.C..

Albert, J. M., and J. Bortnik (2009), Nonlinear interaction of radiation belt electrons with electromagnetic ion cyclotron waves, *Geophys. Res. Lett.*, *36*, L12110, doi:10.1029/2009GL038904.

Clausen, L. B. N., J. B. H. Baker, J. M. Ruohoniemi, and H. J. Singer (2011), EMIC waves observed at geosynchronous orbit during solar minimum: Statistics and excitation, *J.*

Geophys. Res., *116*, A10205, doi:10.1029/2011JA016823.

Furuya, N., Y. Omura, and D. Summers (2008), Relativistic turning acceleration of radiation belt electrons by whistler mode chorus, *J. Geophys. Res.*, *113*, A04224, doi:10.1029/2007JA012478.

Gendrin, R. (1981), General relationship between wave amplification and particle diffusion in a magnetoplasma, *Rev. Geophys. Space Phys. 19*, pages 171-184

Jordanova, V. K., J. Albert, and Y. Miyoshi (2008), Relativistic electron precipitation by EMIC waves from self-consistent global simulations, *J. Geophys. Res.*, *113*, A00A10, doi:10.1029/2008JA013239.

Kasahara, Y., Y. Miyoshi, Y. Omura, O. P. Verkhoglyadova, I. Nagano, I. Kimura, and B. T. Tsurutani (2009), Simultaneous satellite observations of VLF chorus, hot and relativistic electrons in a magnetic storm eerecoveryff phase, *Geophys. Res. Lett.*, *36*, L01106, doi:10.1029/2008GL036454.

Lauben, D. S., U. S. Inan, T. F. Bell, D. L. Kirchner, S. B. Hospodarsky, and J. S. Pickett (1998), VLF chorus emissions observed by Polar during the January 10, 1997 magnetic cloud, *Geophys. Res. Lett.*, *25*, 2995.

Lauben, D. S., U. S. Inan, T. F. Bell, and D. A. Gurnett (2002), Source characteristics of ELF/VLF chorus, *J. Geophys. Res.*, *107*, 1429, doi:10.1029/2000JA003019.

Liu, K., D. S. Lemons, D. Winske, and S. P. Gary (2010), Relativistic electron scattering by electromagnetic ion cyclotron fluctuations: Test particle simulations, *J. Geophys. Res.*, *115*, A04204, doi:10.1029/2009JA014807.

Miyoshi, Y., K. Sakaguchi, K. Shiokawa, D. Evans, J. Albert, M. Connors, and V. Jordanova (2008), Precipitation of radiation belt electrons by EMIC waves, observed from

ground and space, *Geophys. Res. Lett.*, *35*, L23101, doi:10.1029/2008GL035727.

Nunn,D., and Y. Omura (2012), A computational and theoretical analysis of falling frequency VLF emissions, *J. Geophys. Res.* , *submitted*.

Omura, Y., and D. Summers (2006), Dynamics of high-energy electrons interacting with whistler mode chorus emissions in the magnetosphere, *J. Geophys. Res.*, *111*, A09222, doi:10.1029/2006JA011600.

Omura, Y., N. Furuya, and D. Summers (2007), Relativistic turning acceleration of resonant electrons by coherent whistler mode waves in a dipole magnetic field, *J. Geophys. Res.*, *112*, A06236, doi:10.1029/2006JA012243.

Omura, Y., Y. Katoh, and D. Summers (2008), Theory and simulation of the generation of whistler-mode chorus, *J. Geophys. Res.*, *113*, A04223, doi:10.1029/2007JA012622.

Omura, Y., M. Hikishima, Y. Katoh, D. Summers, and S. Yagitani (2009), Nonlinear mechanisms of lower-band and upper-band VLF chorus emissions in the magnetosphere, *J. Geophys. Res.*, *114*, A07217, doi:10.1029/2009JA014206.

Omura, Y., J. Pickett, B. Grison, O. Santolik, I. Dandouras, M. Engebretson, P. M. E. Decreau, and A. Masson (2010), Theory and observation of electromagnetic ion cyclotron triggered emissions in the magnetosphere, *J. Geophys. Res.*, *115*, A07234, doi:10.1029/2010JA015300.

Omura, Y., and D. Nunn (2011), Triggering process of whistler mode chorus emissions in the magnetosphere, *J. Geophys. Res., 116*, A05205, doi:10.1029/2010JA016280.

Pickett, J. S., et al. (2010), Cluster observations of EMIC triggered emissions in association with Pc1 waves near Earth's plasmapause, *Geophys. Res. Lett.*, *37*, L09104, doi:10.1029/2010GL042648.

Rodger, C. J., T. Raita, M. A. Clilverd, A. Seppala, S. Dietrich, N. R. Thomson, and T. Ulich (2008), Observations of relativistic electron precipitation from the radiation belts driven by EMIC waves, *Geophys. Res. Lett.*, *35*, L16106, doi:10.1029/2008GL034804.

Santolik, O., D. A. Gurnett, J. S. Pickett, M. Parrot, and N. Cornilleau-Wehrlin (2003), Spatio-temporal structure of storm-time chorus, *J. Geophys. Res.*, *108 (A7)*, 1278, doi:10.1029/2002JA00979

Shoji, M., and Y. Omura (2011), Simulation of electromagnetic ion cyclotron triggered emissions in the Earth's inner magnetosphere, *J. Geophys. Res.*, *116*, A05212, doi:10.1029/2010JA016351.

Shoji, M., Y. Omura, B. Grison, J. Pickett, I. Dandouras, and M. Engebretson (2011), Electromagnetic ion cyclotron waves in the helium branch induced by multiple electromagnetic ion cyclotron triggered emissions, *Geophys. Res. Lett.*, *38*, L17102, doi:10.1029/2011GL048427.

Summers, D., B. Ni, and N. P. Meredith (2007a), Timescales for radiation belt electron acceleration and loss due to resonant wave-particle interactions: 1. Theory, *J. Geophys. Res.*, *112*, A04206, doi:10.1029/2006JA011801.

Summers, D., B. Ni, and N. P. Meredith (2007b), Timescales for radiation belt electron acceleration and loss due to resonant wave-particle interactions: 2. Evaluation for VLF chorus, ELF hiss, and EMIC waves, *J. Geophys. Res.*, *112*, A04207, doi:10.1029/2006JA011993.

Tsurutani, B. T., and E. J. Smith (1974), Postmidnight chorus: A substorm phenomenon, *J. Geophys. Res.*, *79*, 118.

Wang, Y., W. Gekelman, P. Pribyl, and K. Papadopoulos (2012), Scattering of magnetic mirror trapped fast electrons by a shear Alfvén wave, *Phys. Rev. Lett.*, *108*, 105002.

Figure 1. Configuration of wave magnetic and electric field vectors B_w, E_w, static magnetic field B_0, wavenumber vector k, and parallel and perpendicular velocities $v_\parallel$, $v_\perp$ in the spatial coordinates (x, y, z).

Figure 2. (a) Dispersion relation of EMIC waves, and (b) minimum kinetic energy of resonant electrons.

Figure 3. Trajectories of resonant electrons in (ζ, θ) plane as a solution of the simplified equations of motion with inhomogeneity factors (a) $S = 0$ and (b) $S = -0.4$.

Figure 4. Schematic illustration of frequency variation of the EMIC wave packet at the initial time t_0 and a later time t_1 $(> t_0)$ in red and blue, respectively. A resonant electron passes through the wave packet with $v_\parallel$ $(\gg V_{gt}, V_{gf})$.

Figure 5. Time histories of pitch angles α, trajectories of resonant electrons interacting with an EMIC wave packet with $B_w = 0.009B_{EQ}$ in (θ, ζ) phase space, and distributions F of the resonant electrons in equatorial pitch angles α_{EQ} after the interaction with the wave. The dashed lines indicate the initial distributions. (a) Case A: 0.98 MeV and constant ω. (b) Case B: 3.1 MeV and constant ω. (c) Case C: 0.98 MeV, constant ω, and larger a. (d) Case D: 0.98 MeV and increasing ω. (e) Case E: 0.98 MeV, increasing ω, and larger a.

Figure 6. The similar plots of Cases A-E in Figure 5 with a smaller wave amplitude $B_w = 0.0045B_{EQ}$.

Figure 7. The similar plots of Cases A-E in Figure 6 for electrons with lower initial pitch angles $\alpha = 10 \sim 30$ degrees.

Figure 8. Time histories of (a) pitch angles and (b) variations of kinetic energies of trapped electrons in red and untrapped resonant electrons in blue with different initial pitch angles $\alpha = 10, 20, 30, 40, 50, 60, 70$ degrees for Case E with $B_w = 0.009B_{EQ}$.

Table 1. Input Parameters

Parameter		Normalized Value	Real Value
time step	Δt	$0.2/\ \Omega_{e0}$	4.7×10^{-6} s
grid spacing	Δz	$1.0c/\Omega_{e0}$	7.0 km
electron cyclotron frequency at equator	f_{ce}		6.8 kHz
proton cyclotron frequency at equator	f_{cH}		3.7 Hz
electron plasma frequency at equator	f_{pe}	$18 f_{ce}$	120 kHz
electron density at equator	n_e		178 /cc
proton density at equator	n_H	$0.81\ n_e$	144 /cc
helium density at equator	n_{He}	$0.095\ n_e$	17 /cc
oxygen density at equator	n_O	$0.095\ n_e$	17 /cc
angular electron plasma frequency at equator	ω_{pe}	$18\Omega_{e0}$	7.5×10^5 rad/s
coefficient of parabolic magnetic field	a	$(0.8, 3.0) \times 10^{-7}\Omega_{e0}^2/c^2$	
wave frequency	f	$0.46 - 0.76 f_{cH}$	1.7 - 2.8 Hz
wave amplitude	B_w	$0.009, 0.0045 B_{EQ}$	2.2, 1.1 nT
initial wave packet length		$1000\ c/\Omega_{e0}$	7000 km

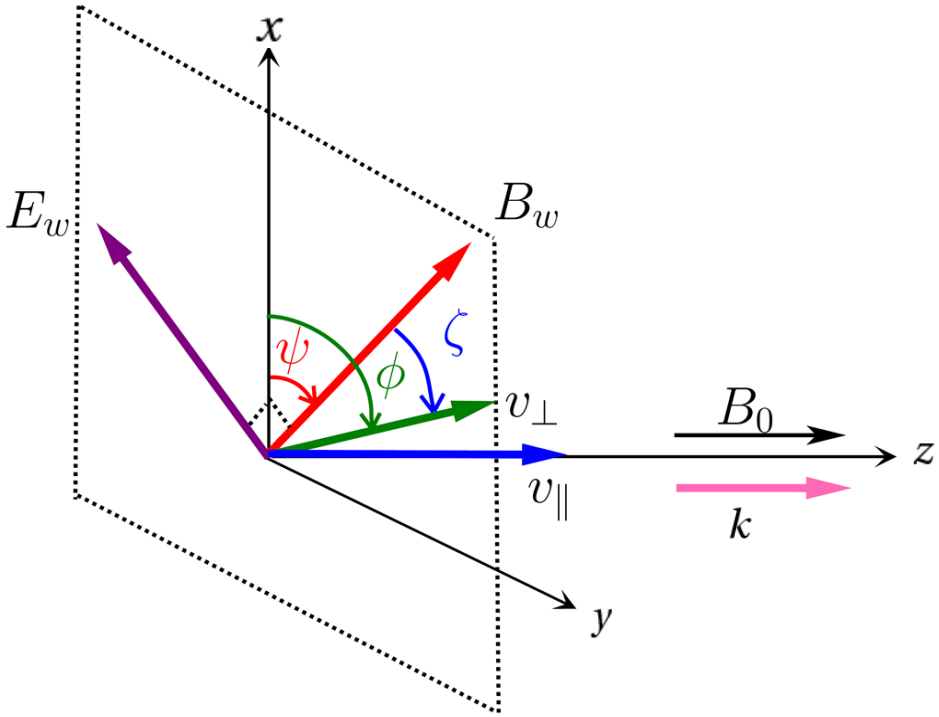

Figure 1. Configuration of wave magnetic and electric field vectors $\boldsymbol{B}_w$, $\boldsymbol{E}_w$, static magnetic field $\boldsymbol{B}_0$, wavenumber vector $\boldsymbol{k}$, and parallel and perpendicular velocities $\boldsymbol{v}_\parallel$, $\boldsymbol{v}_\perp$ in the spatial coordinates (x, y, z).

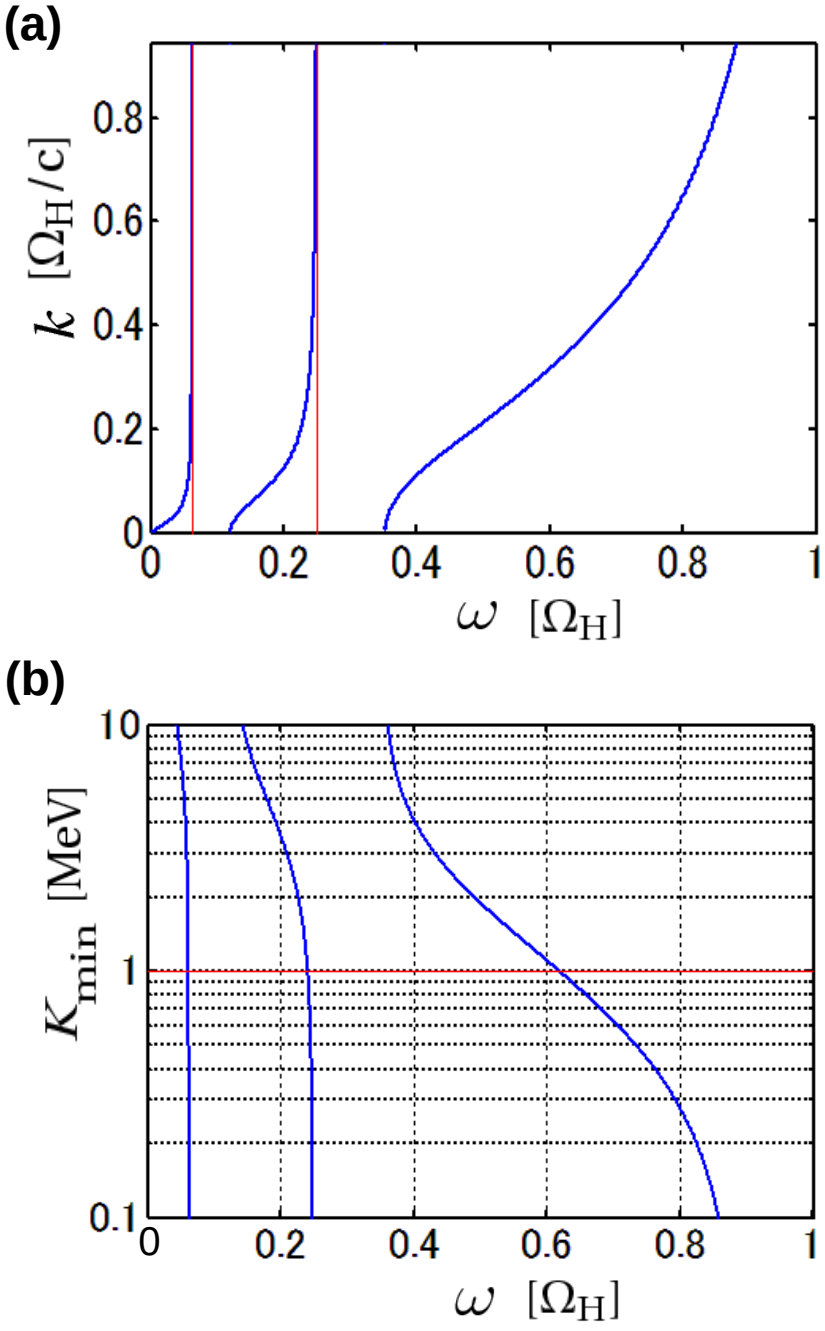

Figure 2. (a) Dispersion relation of EMIC waves, and (b) minimum kinetic energy of resonant electrons.

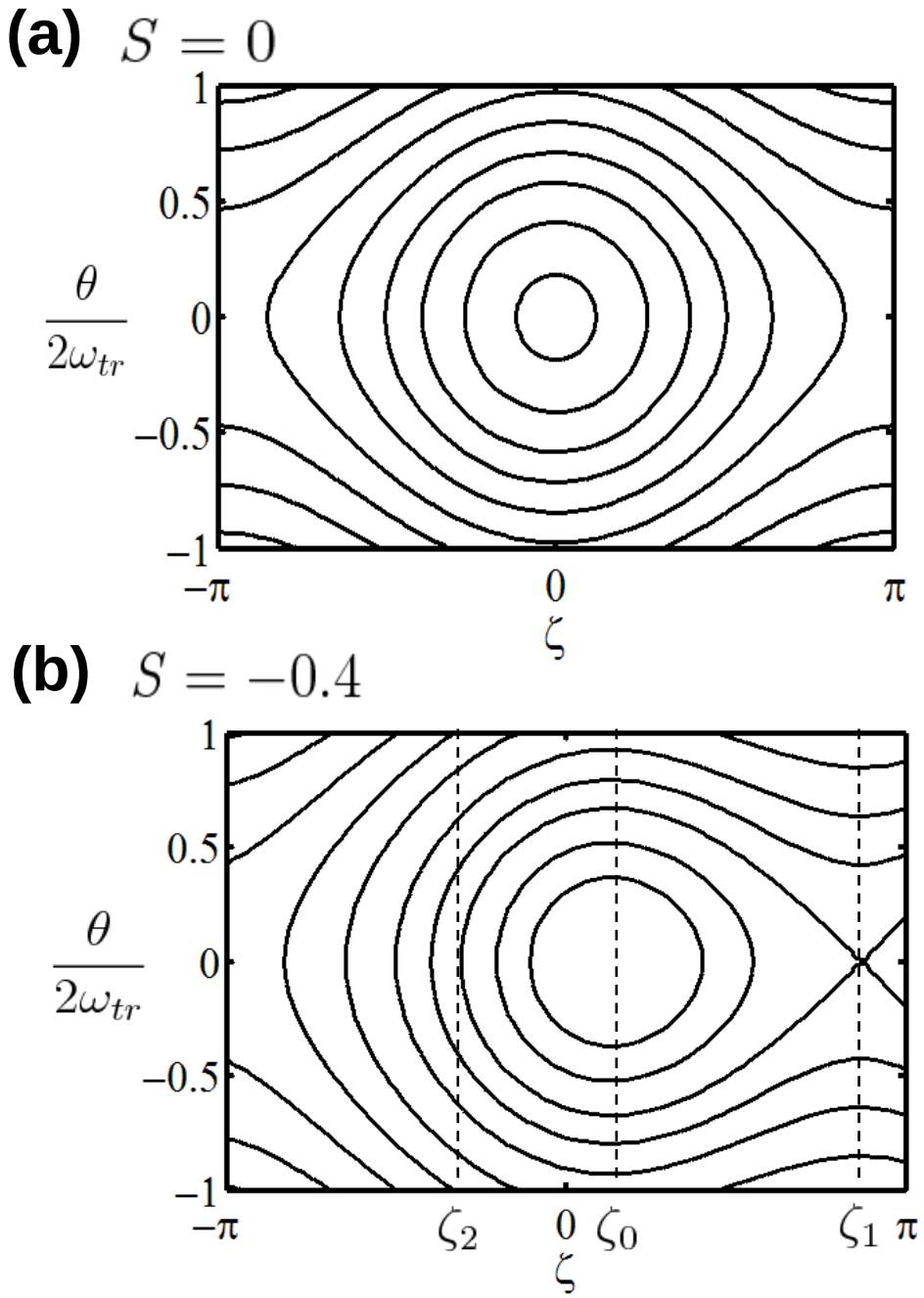

Figure 3. Trajectories of resonant electrons in (ζ, θ) plane as a solution of the simplified equations of motion with inhomogeneity factors (a) $S = 0$ and (b) $S = -0.4$.

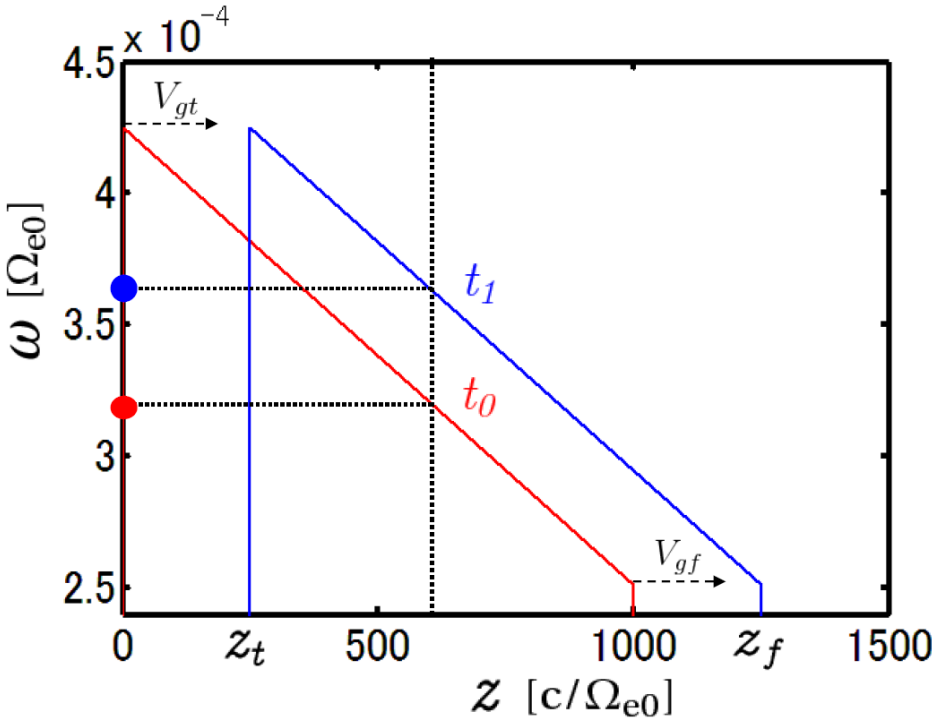

Figure 4. Schematic illustration of frequency variation of the EMIC wave packet at the initial time t_0 and a later time t_1 ($> t_0$) in red and blue, respectively. A resonant electron passes through the wave packet with $v_{\parallel}$ ($\gg V_{gt}, V_{gf}$).

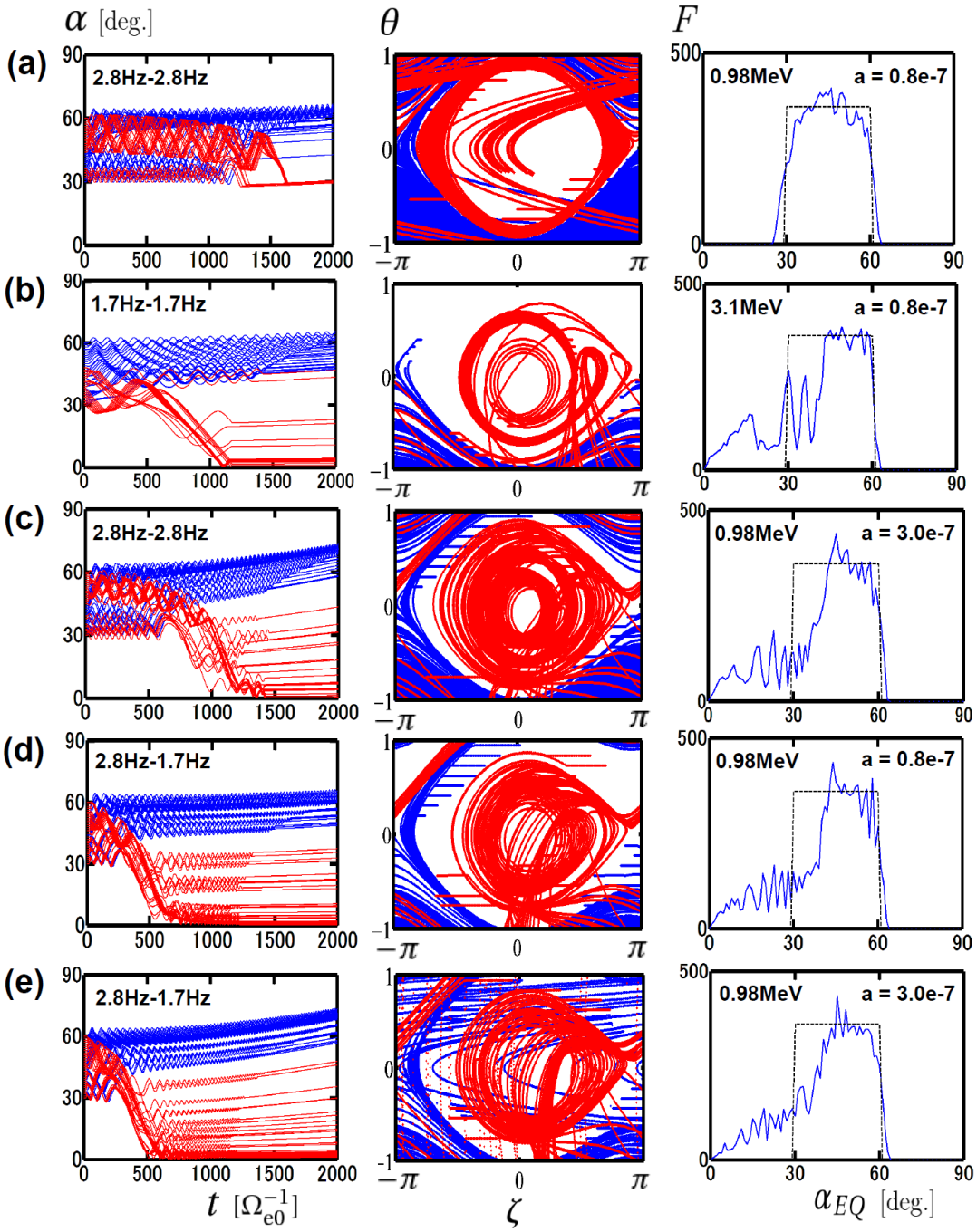

Figure 5. Time histories of pitch angles α, trajectories of resonant electrons interacting with an EMIC wave packet with $B_w = 0.009 B_{EQ}$ in (θ, ζ) phase space, and distributions F of the resonant electrons in equatorial pitch angles α_{EQ} after the interaction with the wave. The dashed lines indicate the initial distributions. (a) Case A: 0.98 MeV and constant ω. (b) Case B: 3.1 MeV and constant ω. (c) Case C: 0.98 MeV, constant ω, and larger a. (d) Case D: 0.98 MeV and increasing ω. (e) Case E: 0.98 MeV, increasing ω,

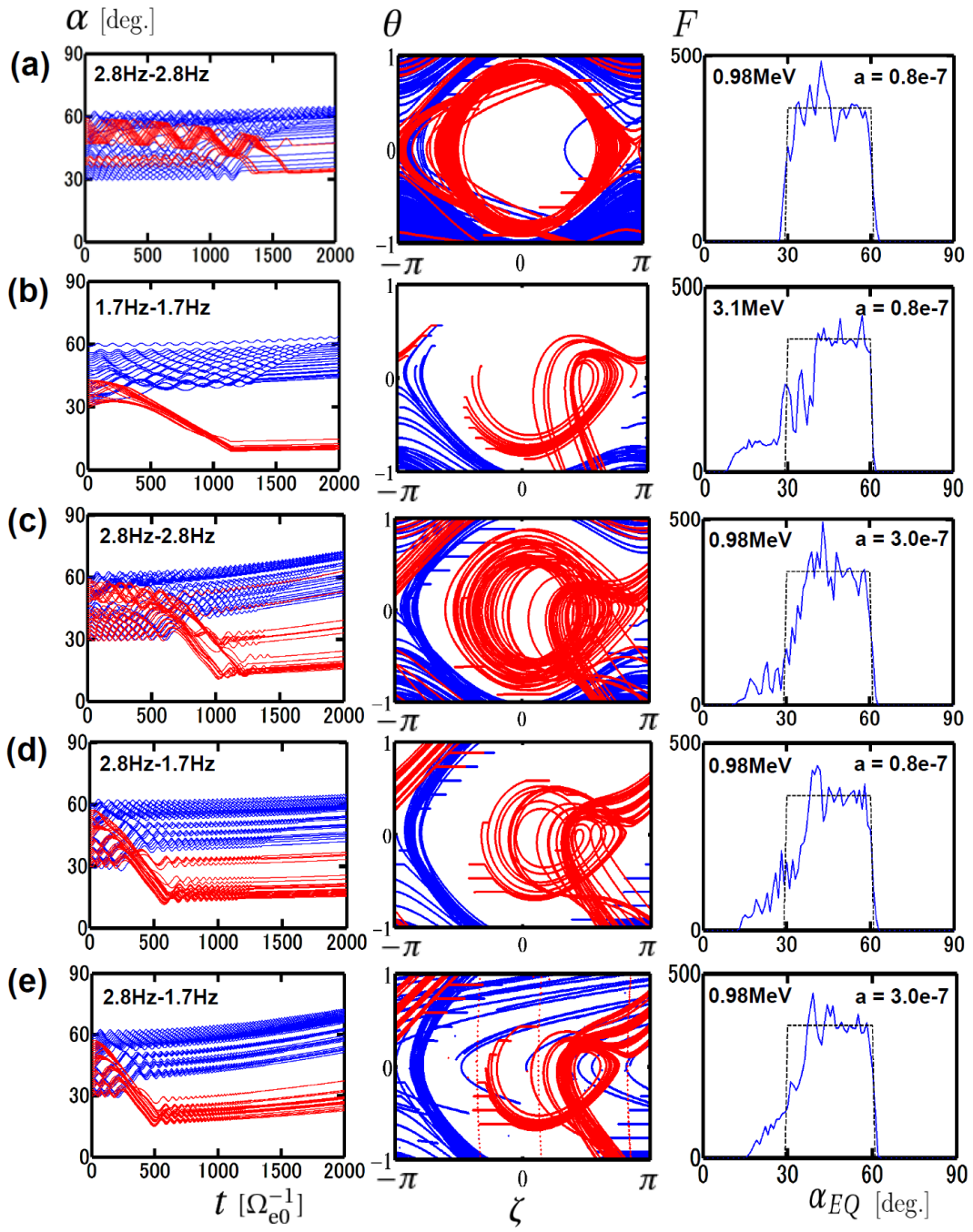

Figure 6. The similar plots of Cases A-E in Figure 5 with a smaller wave amplitude $B_w = 0.0045 B_{EQ}$.

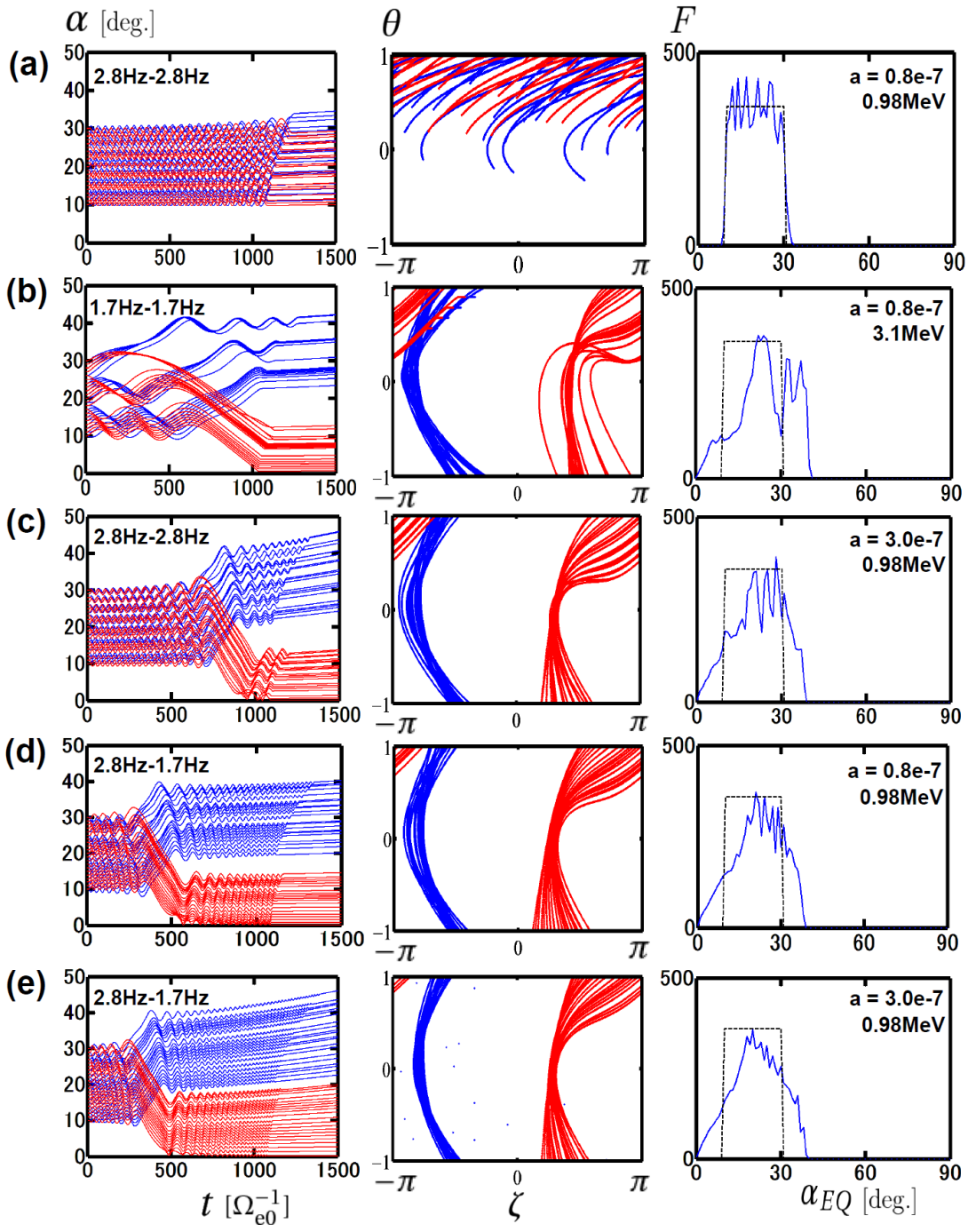

Figure 7. The similar plots of Cases A-E in Figure 6 for electrons with lower initial pitch angles $\alpha = 10 \sim 30$ degrees.

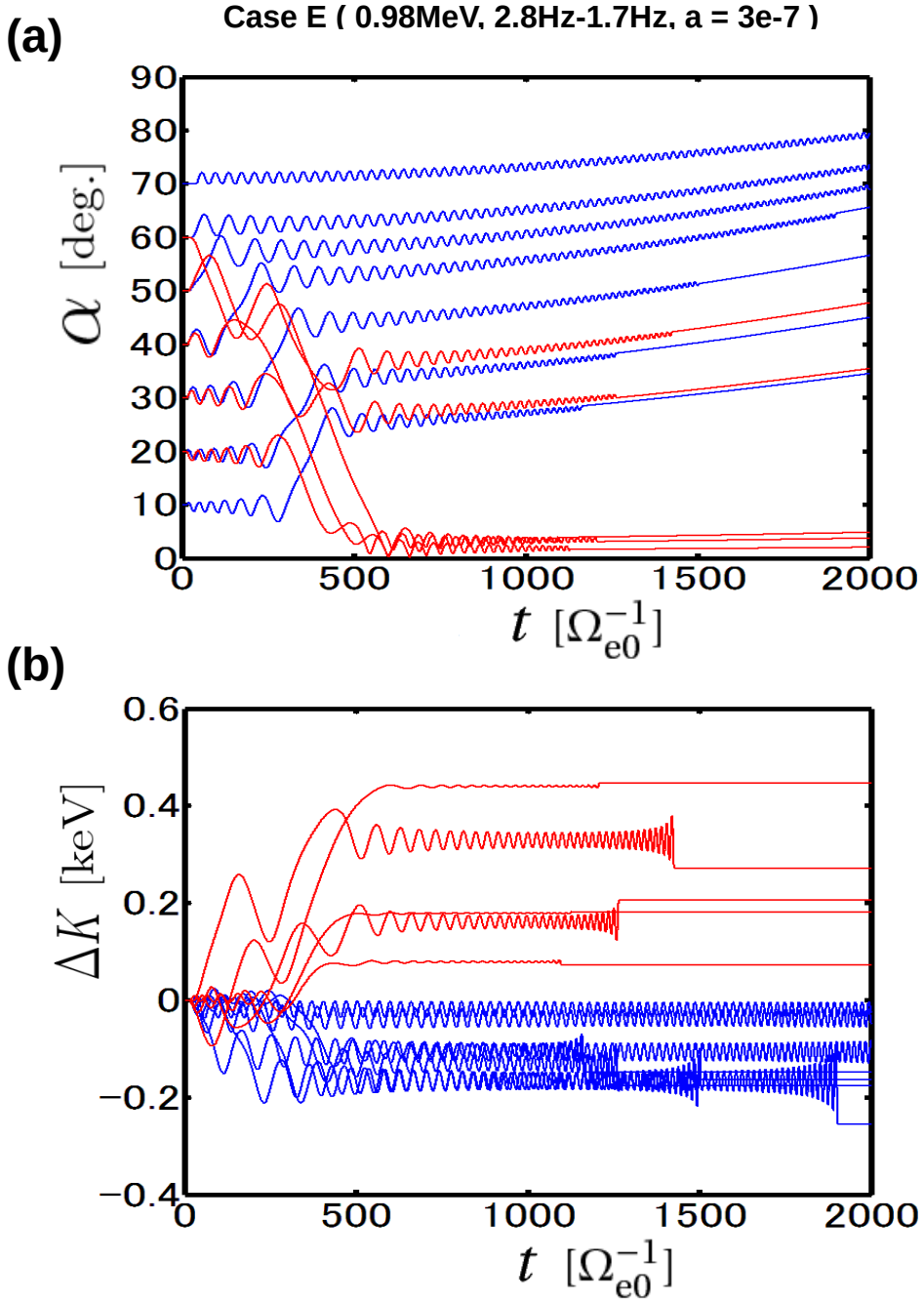

Figure 8. Time histories of (a) pitch angles and (b) variations of kinetic energies of trapped electrons in red and untrapped resonant electrons in blue with different initial pitch angles $\alpha = 10, 20, 30, 40, 50, 60, 70$ degrees for Case E with $B_w = 0.009 B_{EQ}$.